GROUND TRUTH LOCATIONS USING SYNERGY BETWEEN REMOTE SENSING AND SEISMIC METHODS - APPLICATION TO CHINESE EARTHQUAKES

Chandan K. Saikia[1], Ji Chen[2], Gene A. Ichinose[1], Donald V. Helmberger[2], Ali O. Konca[2], and Mark Simons[2]

URS Group, Inc[1]; California Institute of Technology[2]

Sponsored by Department of Energy
Office of Nonproliferation Research and Engineering
Office of Defense Nuclear Nonproliferation

Contract No. DE-AC52-03NA995051

ABSTRACT

The primary objective of this study is to establish ground truth locations of moderate to large magnitude earthquakes ($4.5 \leq M_w \leq 8$) occurring in China using a synergy between seismic and synthetic aperture radar interferometric methods. To this end, we have analyzed both seismic waveforms and relevant InSAR data for the Tibet (Manyi) earthquake (97/11/08, origin time: 10h02m, latitude: 35.069˚E, longitude: 87.325˚N, PDE; and M_w=7.5) and its large aftershock (01/03/05, origin time: 15h50m, latitude: 34.369˚N, longitude: 86.902˚E, and M_w=5.7). In addition to these events, we have also successfully analyzed similar data from another earthquake in northeastern China (98/01/10, origin Time: 03h50m, latitude: 41.11˚N, longitude: 114.55˚E, and M_w=5.7). For this last event, we modeled its teleseismic P waves and long-period regional waveforms separately and established a depth of 7 km, consistent with the depth estimates reported in the EHB and ISC catalogs (within ±2km). Our estimated depth is off by tens of km from other catalogs including the value reported in the Chinese catalog. We have further analyzed the radar data from frame 2772 on tracks 304 and 32, and geo-deformation from this earthquake could easily be delineated in the processed interferograms. For the 1997 M_w 7.5 Manyi earthquake, we established kinematics rupture model using teleseismic P waves (14 stations) and SH waves (9 stations). Seismic data could be modeled using a vertical fault plane striking toward 80˚N, but their complex waveform characteristics required three major sub-events. The slip in the first 4 sec from the first event was very small, which was followed primarily by a pure strike-slip sub-event and occurred east of the hypocenter rupturing for about 6 sec with a peak slip around 7m. The second sub-event occurred 40 km west of the hypocenter and ruptured following 15 to 25 seconds of the first event. The third event occurred 80 km west of the hypocenter about 45 sec later. The average rupture velocity is 2.1 km/sec, which is about 60% of the shear velocity. A slip model was also built based on the geo-deformation obtained by processing InSAR data from frame 2889 on tracks 33, 76, and 305. The major pattern of slip distribution is consistent with the seismic analysis, but the slip distribution requires about 33 km spatial shifting to 35.30˚N and 87.55˚E. This new slip model is being used to refine the hypocenter on the fault using a procedure recently developed by Chen et al. (2004). The seismic study pertaining to its aftershock has indicated that it is a shallow event and we have ordered its radar data only recently. We further completed regional and teleseismic modeling, including the prediction of the static wavefield, for a M_w 6.4 earthquake (98/08/27, 09h03m34.7s) in southern Xinjiang Province, which indicates that it must have produced surface deformation that will be discernable in satellite data. These new locations will allow a high-quality calibration of a large area around the epicenters using arrival times for various seismic phases that are available for these two events from many stations of the Chinese National Network.

OBJECTIVES

One of the most important problems in seismic monitoring is in determining ground truth (GT) locations so that the events can be used for calibration. Usually, large explosions provide the best GT location with error in the order of 1 km, but they are limited and one must rely primarily on earthquake data to extend the geographical coverage. Geodetic data, in the form of Synthetic Aperture Radar Interferometry (InSAR) measurements, provide much needed help in this process under some circumstances. The overall goal of this ongoing study to utilize geodetic data to establish high quality locations for shallow and moderate-sized earthquake in Asia and North Africa in conjunction with seismic methods to validate ground truth (GT) location results. The work concentrates on events in North Africa (Algeria, Libya, Morocco, and Egypt), southwest Asia (Iraq and Iran, including China) and the Korean Peninsula. One of the major objectives of this study is to develop schemes to ascertain the location of rupture initiation on a given fault associated with large earthquakes. In this presentation, we will discuss earthquakes occurring in China, which have potential to become candidates for such GT events.

RESEARCH ACCOMPLISHED

November 8, 1997 (M_w 7.6) Tibet (Manyi) Mainshock

Our initial thrust here is in development of schemes that integrate both seismic and satellite data in order to establish the GT locations of large earthquakes. The earthquakes of magnitude greater than 6 at shallow depths provide strong co-seismic deformation that is easily discernable in satellite data, but unfortunately are difficult for establishing their epicenters. However, co-seismic deformation can be inverted for a dislocation fault model and the seismic data can then be inverted for a dislocation fault model and the seismic data can be used to establish the time delays of these slip elements on the fault. This approach proved highly effective in the study of the Chi Chi earthquake (Ji et al., 2004).

In this study, we demonstrate the resolving power of InSAR in conjunction with seismic data for the November 8, 1997 M_w 7.6 Manyi (Tibetan) earthquake. This event occurred along the Kun Lun fault as displayed in Figure 1. The fault that ruptured has been studied by Tapponier and Molnar (1977) and portion of it ruptured earlier in 1973. Three epicenters for the main event were reported; two based on the teleseismic data (Centroid Moment Tensor, USGS) and one based on the regional travel time data as published by the Chinese Seismological Bureau (CSB), Beijing. The fault breakage outlined in Figure 1 is discussed in Peltzer et al. (1999).

Modeling of the Teleseismic Data

We used a waveform inversion procedure developed by Ji et al. (2002a,b) that uses wavelet transforms to model the P and S data. The slip model developed based on the teleseismic P waves assuming the location from the Chinese Digital Seismograph Network (CDSN) as a rupture initiation point, including the linear strike orientation (W18°N) of the inferred fault, are displayed in the top panel of Figure 2. We used P waves from 14 and SH waves from 9 teleseismic stations to establish its kinematics rupture process. Seismic data seemed consistent with a vertical fault striking toward 80˚N, but the complex waveform characteristics in observed data required three major sub-events. The slip in the first 4 sec from the first event was very small, which was followed primarily by a pure strike-slip sub-event and occurred east of the hypocenter rupturing for about 6 sec with a peak slip around 7m. The second sub-event occurred 40 km west of the hypocenter and ruptured following 15 to 25 seconds of the first event. The third event occurred 80 km west of the hypocenter about 45 sec later. The average rupture velocity is 2.1 km/sec, which is about 60% of the shear velocity. The event based only on the data shown in Figure 2 has a large asperity near the CDSN epicenter with nearly pure strike-slip vectors although a second energy release occurs to the east separated by about 50 km. Nearly all of the slip occurs above the depth of 15 km. This slip distribution is quite compatible with those of Velasco et al. (2000).

InSAR Results

The InSAR data used in conjunction with the fault breakage geometry is given in the middle panel in Figure 2. Using ROIPAC, we processed radar data from frame 2889 on tracks 33, 76, and 305 using ROIPAC jointly developed at Jet Propulsion National Laboratory and California Institute of Technology. The slip appears to be more concentrated in length, but deeper in extent; its signature appears different from the seismic model. The distributed slip occurs along six segments with slight changes in rotation as indicated in Figure 1. The slip vectors indicate some thrust motion near

the CDSN epicentral location, which appears to be associated with the rupturing of the asperity on the right. Since it is a big earthquake, we can combine this data with the seismic data to establish a better location of the epicenter.

Synergy of Seismic and InSAR Results

The combined inversion produces a very good fit to all data (discussed later) with a complex looking picture (bottom panel in Figure 2), but its major feature is similar to the slip model developed based on the InSAR data alone. The dominate motions and geodetic filed occurs over a zone of about 50 km, which appears to be well resolved. The pattern to the east seems too complicated and may be produced by forcing the seismic data to fit. Note the shallow and deep pattern, which produces some interference patterns in the waveform fits. The most important change in result in this new position of the epicenter, which moved 20 km to the west and to a depth of 16 km.

Prediction of Regional Waveforms

One of the biggest advantages of this inversion method is the simplicity of our time history, which is essentially one parameter

$$S(t) = \frac{1-\cos(2\pi t/r)}{r} \qquad 0 < t < r$$

where $\dot{S}(t)$ is the derivative of the rise-time, after Cotton and Campillo (1995). This assumption greatly reduces the number of the parameters used in the inversion and allows predictions (Ji et al., 2004). For example, the predictions at stations situated on the Tibetan Plateau are displayed in Figure 3. These fits are based on absolute travel times and amplitudes which appear to agree very well with the crustal model of the region.

Foreshock Problem

The location in Figure 2 (bottom panel) is controlled by the main rupture and not affected by weak precursor, which has been reported in *ACTA Seismologica Sinica* (V21, No 5, Sept 1999). They conclude that a small foreshock occurred roughly 5 seconds before the main event based on the CDSN data. This small event can, also, be seen at the teleseismic distances (Figure 4). We present these panels where the beginning motions have been enhanced on the left. The middle column displays observations from several stations WRAB-YSS that start about 5 seconds early ranging in azimuth (133° to 56°). This weak motion appears to come from the same location as the mainshock and is probably a typical initiation event for many of the events that followed.

The location suggested by Velasco et al. (2000) is halfway between our preferred (Figure 1) and the CDSN (35.19°N, 87.43°E), which is in good agreement (roughly 10 km different). We plan to examine the regional data in more detail in future.

March 5, 2001 (M_w 5.7) Tibet Aftershock

The March 5, 2001 (15h:50m:07.63s, 34.258°N 86.860°E, 38.9 km, M_w=5.7) earthquake is the largest aftershock of the Tibet (Manyi) earthquake. Its depth is an unresolved parameter and is deeper than 20 km, as reported in all earthquake catalogs. To ascertain its depth, we analyzed its teleseismic P waves (often noisy at all stations) and found the event to have a complex source process, involving several sources like the mainshock. Teleseismic modeling (Figure 5) shows that its depth can be anywhere between 2 and 6 km. The focal mechanisms determined at these various depths (h<6 km) have the same strike as the mainshock (340°) and similar dip and rake angles. Modeling using the source at deeper depths resulted in focal mechanism that indicates that the earthquake was caused by movement across a tensional fault. Regional seismograms have good signal-to-noise ratios. Preliminary modeling of these regional data indicates that it is indeed a shallow earthquake. In addition, numerical calculation of the static wavefield based on the focal mechanism presented in Figure 5 suggests that its surface deformation will be discernable in satellite data. We will receive its satellite data soon from EURIMAGE and analyze both the seismic and satellite data together to establish its ground truth location.

January 10, 1998 (M_w 5.7) North East China Earthquake

Next, we examined earthquakes occurring in the northeast part of China. We have successfully examined both seismic and satellite data for the January 10, 1998 earthquake (ISC: 03h: 50m:37.88s, 41.1131°N 114.5010°E, h=4.8 km, M_w 5.7). The in-country scientists in China have also located this earthquake using the CDSN travel times and determined its epicentral location at latitude 41.14°N and longitude 114.52°E, similar to the ISC epicenter. The CDSN depth is at 17 km. We modeled its teleseismic P waves and long-period regional waveforms separately and established a depth of 7 km (Figure 6), consistent with the depth estimates reported in the EHB and ISC catalogs (within ±2km). Our estimated depth is off by tens of km from other catalogs, including the depth reported in the CDSN catalog. It is also recorded at 12 regional (R<13.5°) and 16 upper-mantle (15°<R<30°) stations with good signal-to-noise ratios. We also acquired radar data relevant to this earthquake from frame 2772 on tracks 304 and 32 acquired on 97/09/23 and 98/05/26. The interferograms have been processed where we could easily delineate four fringes associated with the surface deformation caused by this earthquake. The horizontal extent of these fringes is from 41.1209°N/114.426°E (lat/lon) to 41.14°N/114.519°E and of the vertical extent is from 41.0926°N/114.467°E to 41.1967°/114.476°E.

The next step in this analysis is to model the delineated surface deformation field together with the regional and teleseismic waveforms to conclusively establish the ground truth location of this earthquake. We collected travel-time data from 85 CDSN stations within 30° for this earthquake which will provide basis for reliable source specific station corrections (SSSCs) for the calibration of China. Additionally, many earthquakes have occurred in northeast China in the proximity of this earthquake. Hence, these SSSCs will enable us to provide reliable locations for these others events (Saikia et al., 2003).

August 27, 1998 (M_w 6.4) Southern Xinjian Province, China Earthquake

Based on the seismic data analysis, we also identified an earthquake that occurred in the southern Xinjiang Province, China on August 27, 1998 (09h03m:34.7s, 39.67°N 77.31°E, h=23 km, Ms 6.4, CDSN). Both regional and teleseismic waveforms of this earthquake were modeled and are consistent with a shallow depth (Figure 7). The top right panel shows agreement between regional data and synthetic seismograms and the bottom panel shows the same for the teleseismic P waves. Teleseismic P waves were modeled using the "Kikuchi method". Like the other earthquakes, this event is also complex and required multiple sources as shown in the top right panel to fit both regional and teleseismic observations. An initial calculation of the static deformation along the vertical line-of-sight has suggested that this earthquake must have produced surface deformation, which should be discernable in the satellite data.

CONCLUSIONS AND RECOMMENDATAIONS

The overall objective of this three-year study is to concentrate on events in North Africa (Algeria, Libya, Morocco, and Egypt), southwest Asia (Iraq and Iran, including China) and the Korean Peninsula. However, this study is primarily focused on the earthquakes occurring China because of the availability of travel-time data from the Chinese network stations. This study shows that the travel-time data from the Chinese Digital Seismograph Network (CDSN) have great promise for analyzing both the seismic and satellite data together towards establishing ground truth locations for some moderate-sized Chinese earthquakes (M_w>5.5). In areas where such seismic network stations will be sparse or inaccessible, such an effort may encounter difficulties.

We analyzed satellite data and successfully identified surface deformation for two earthquakes. Of these, one is the large November 8, 1997 Tibet (Mayni) earthquake. This is a complex earthquake and consists of several events. Several investigators have analyzed this event and the initial locations presented in these studies differ. By combining both seismic and InSAR data, we established a location that differs from Velasco et al. (2000, Figure 1). Because of this variation, we are performing a sensitivity study to establish the level of uncertainties involved in each of these locations.

Surface deformation was distinctly delineated in satellite data relevant for the January 10, 1998 northeast China earthquake.

Seismic analysis has shown that many earthquakes, which are reported to have occurred at depths, are actually shallow. In light of this observation, we need to continue modeling of both regional and teleseismic data of more earthquakes to

establish ground truth for extending the geographical coverage in China. Our next effort will be to extend these studies to earthquakes occurring in the North Africa and Korean Peninsula.

REFERENCES

Chen, Ji., Wald, D. J., and Helmberger, D. V. (2002a). Source description of the 1999 Hector Mine, California earthquake; Part I: Wavelet domain inversion theory and resolution analysis, Bull Seismol. Soc. Am., 92, 1192-1207.

Chen, Ji., Wald, D. J., and Helmberger, D. V. (2002b). Source description of the 1999 Hector Mine, California earthquake; Part II: Complexity of slip history, Bull. Seismol. Soc. Am., 92, 1208-1226.

Chen, Ji., Helmberger, D. V., Wald, D. J. and Ma, K F. (2003). Slip history and dynamic implications of the 1999 Chi-Chi Taiwan, earthquake, J. Geophys. Res., V108, NO B9, 2412, doi:10,1029.2002JB001764.

Chen Ji., Helmberger, D. V., and Saikia, C. K. (2004). Refined locations using InSAR and seismic waveforms, J. Geophys. Res. Lett. (submitted).

Cotton, F., and Campillo (1995). Frequency domain inversion of strong motions: application to 1992 Landers earthquake, J. Geophys. Res., 100 (B3), 3961-3975.

Peltzer, G., Crame, F., and King., G. (1999). Evidence of non-linear elasticity of the crust from the Mw 7.6 Manyi (Tibet) earthquake, Science, 286, 272-276.

Saikia, C. K., R. Lohman, G, Ichinose, and M. Simons (2003). Ground truth location using a synergy between InSAR and seismic methods, 25th Seism. Res. Rev., Nuclear Explosion Monitoring: Building Knowledge Base, Sept 23-25, p324-333.

Tapponier, P. and Molnar, P. (1977). Active faulting and tectonics in China, J. Geophys. Res., 82, 2905-2930.

Velasco, A. A, Ammon, C. J., and Beck, S. L. (2000). Broadband source modeling of the November 8, 1997 Tibet (Mw 7.5) earthquake and its tectonic implications, J. Geophys. Res., V105, B12, 28,065-28,080.

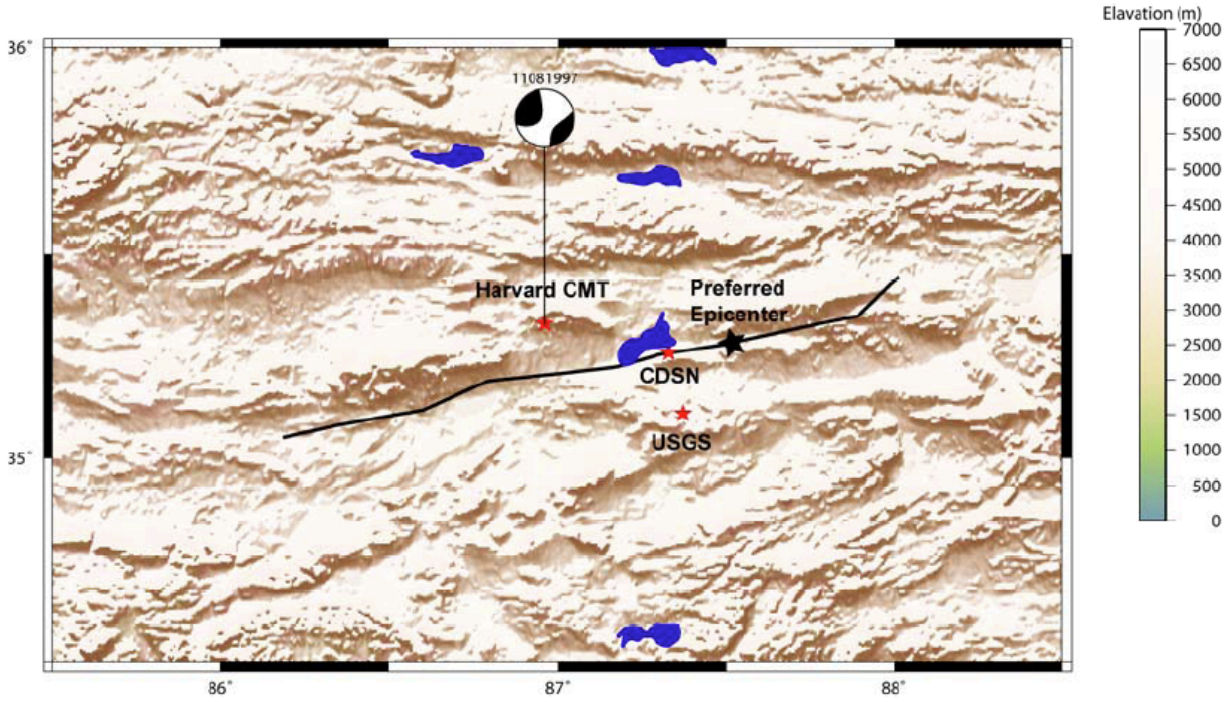

Figure 1. Map with proposed epicenters in red along with our preferred location for the November 8, 1997 Tibet (Mayni) earthquake. The fault breakage is indicated with the heavy dark line.

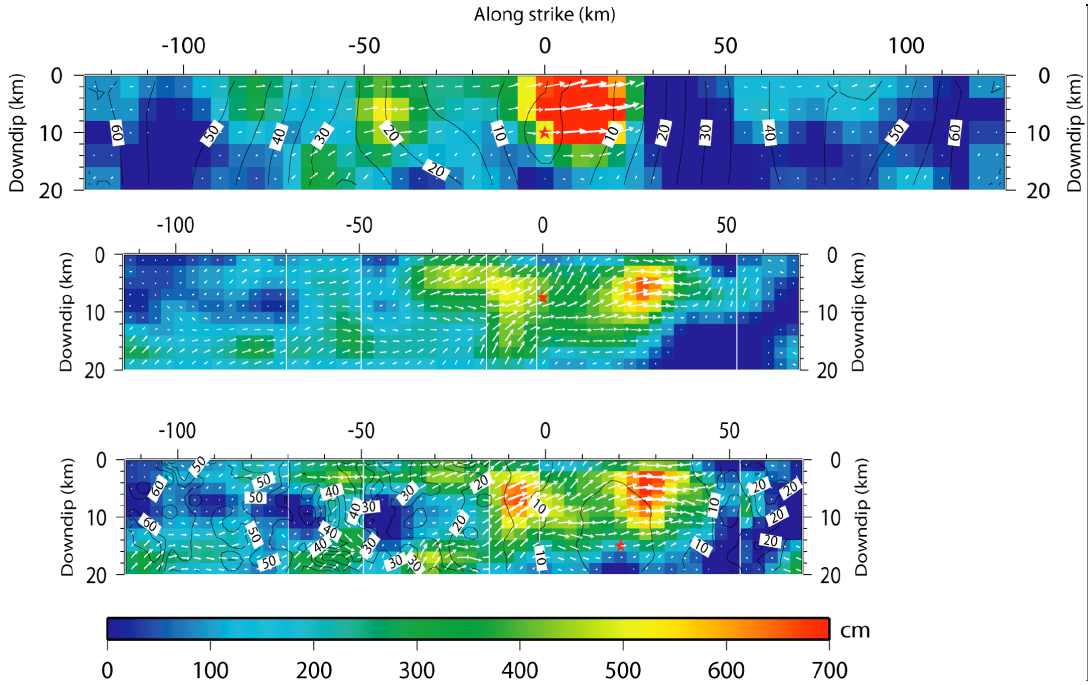

Figure 2. Three panels of slip distributions: top (teleseismic waveforms only), middle (geodetic only, InSAR), and bottom (combined teleseismic and InSAR). Contour lines are included indicating the positions of the rupture front as a function of time after onset. Note that the location of the CDSN epicenter has been shifted 20 km to the right in the bottom panel.

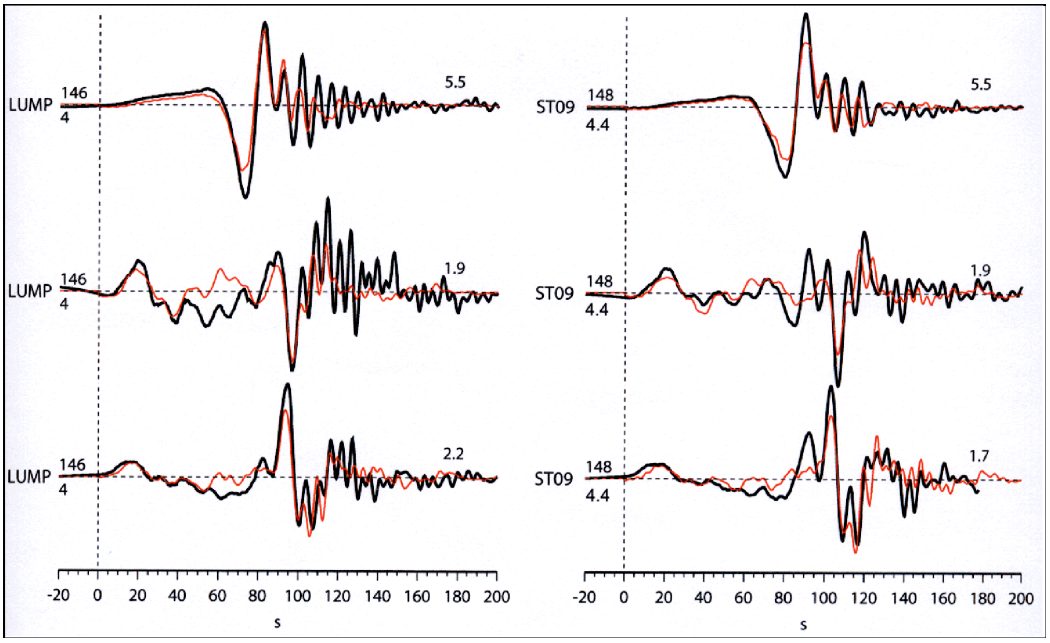

Figure 3. Predictions of synthetics using the combined slip model (InSAR and Teleseismic) along with observations at two PASSCAL stations (INDEPTH III) as given at IRIS stations. They are located about 4 degrees (lower number) and at azimuths given in the top number.

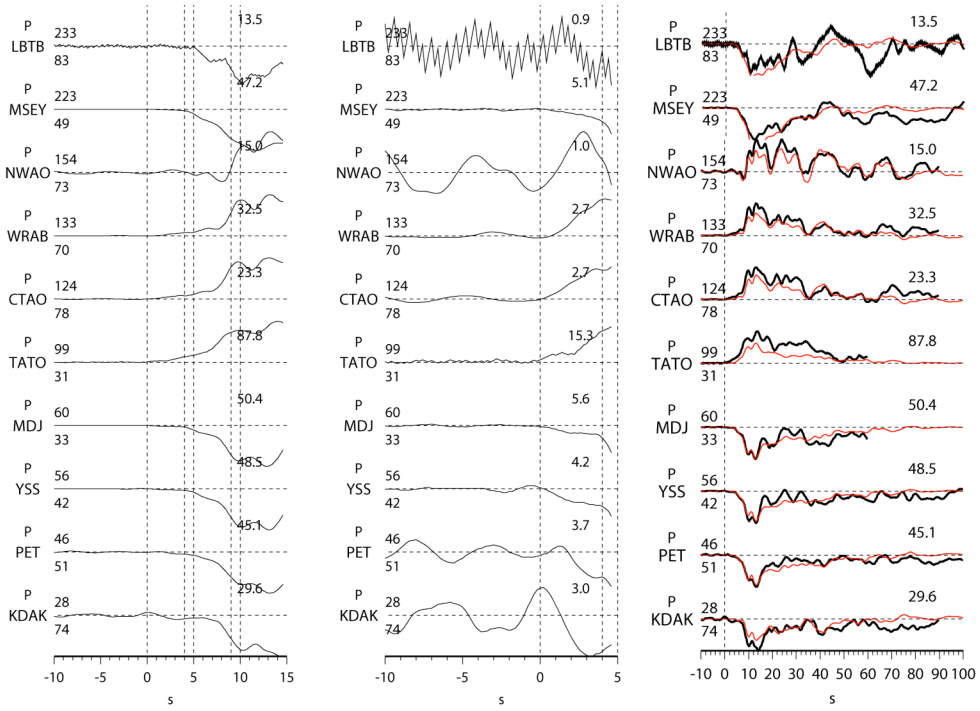

Figure 4. The fits of teleseismic P waveform with the synthetics predicted using the combined slip model (InSAR and teleseismic). Upper number gives the azimuths and lower number the distances. Columns on the left display blow-ups, all aligned on the origin time of the CDSN location. Note the weak onset starting at WRAB.

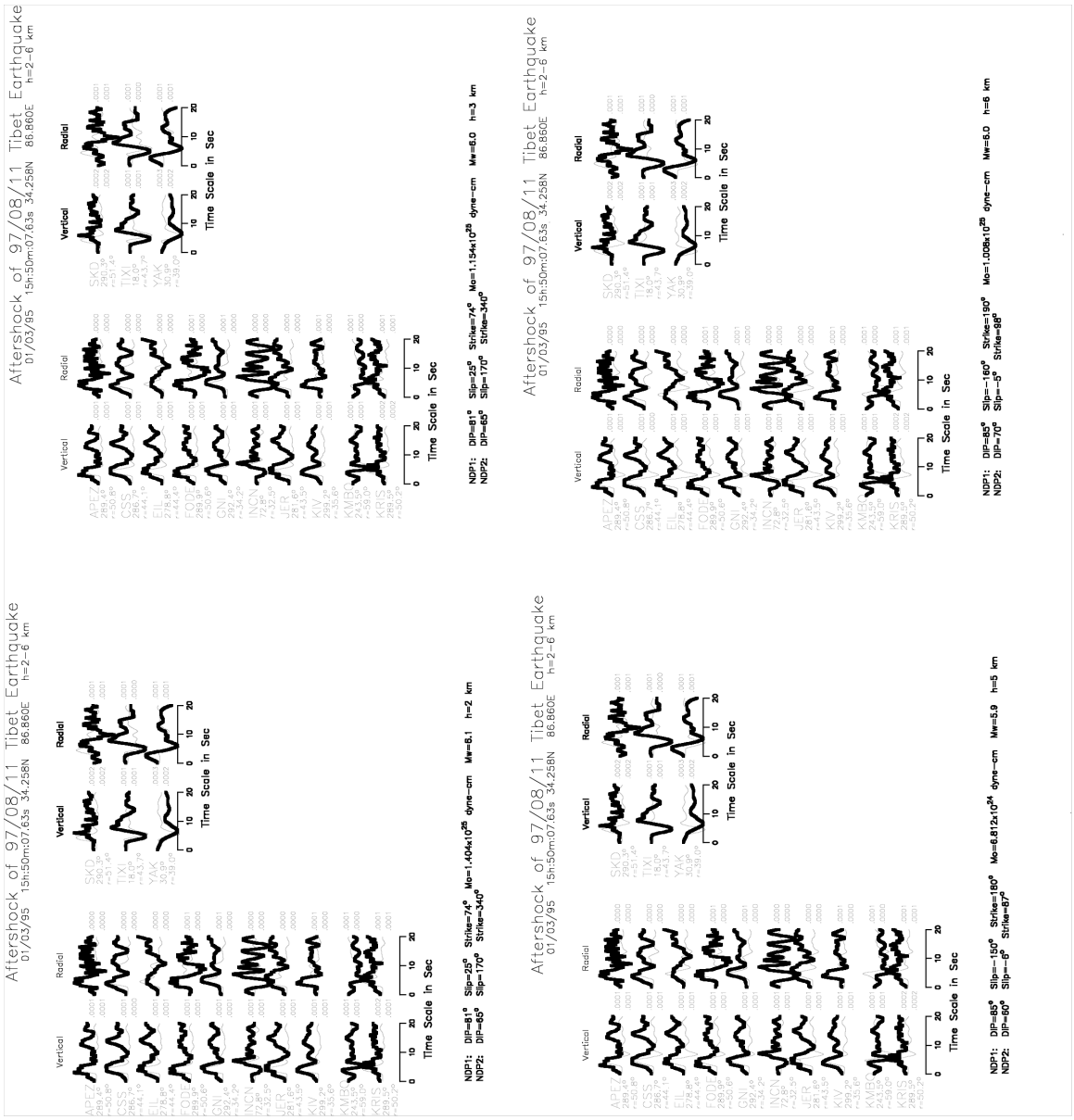

Figure 5. Modeling of teleseismic P waves recorded from the March 5, 2001 in Tibet for a suite of depths and is the largest aftershock of the 1997 Tibet (Mayni) earthquake. We have used a single point source, which is the reason for some mismatch between the synthetics and observations. Based on this modeling study, the earthquake has occurred at a depth shallower than the reported catalog depths.

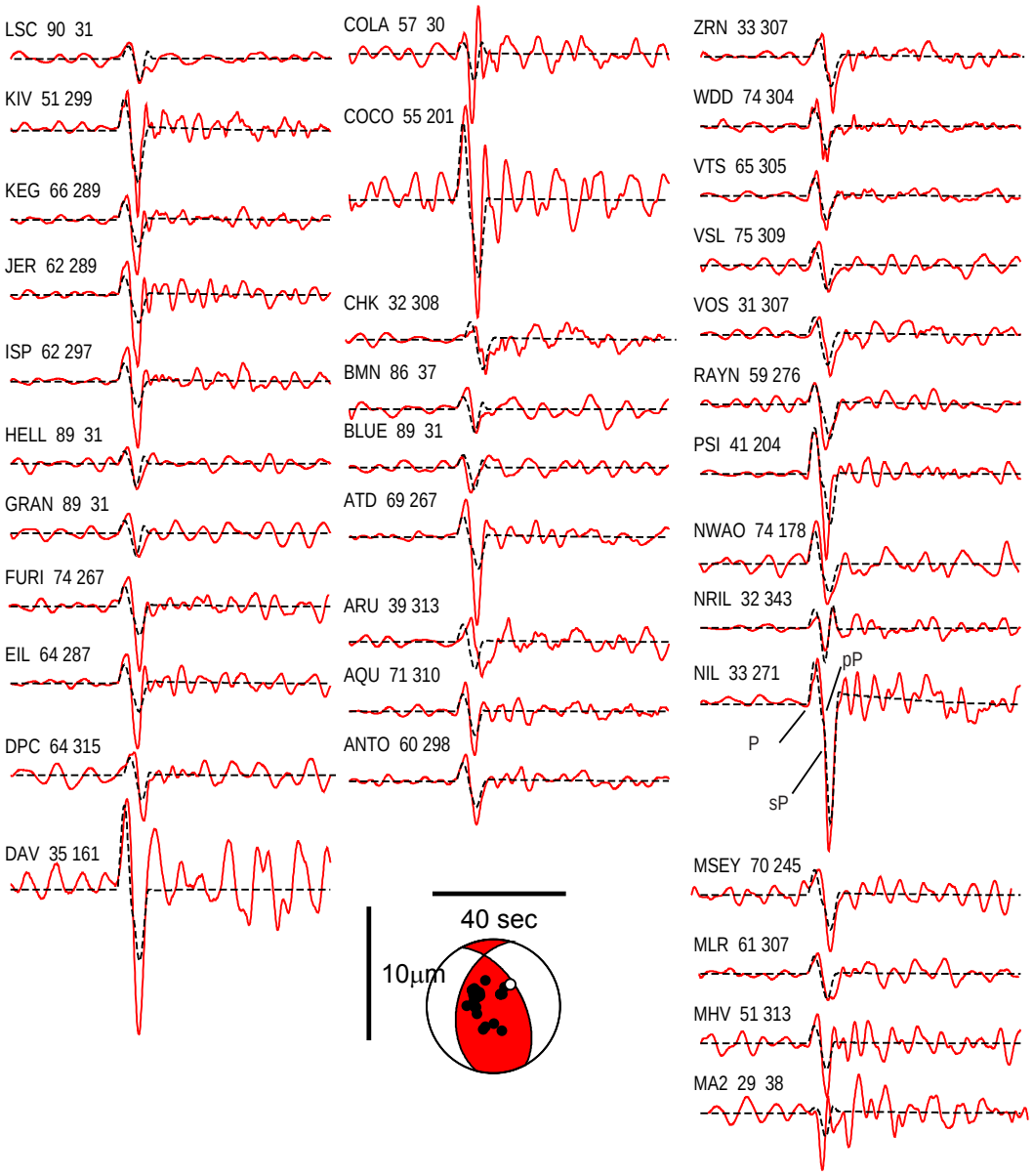

Figure 6. Modeling of teleseismic P waves recorded from the January 10, 1998 North East China earthquake using Green's functions computed for a source at 7 km depth. Also shown is the interference of depth phases (pP and sP) with the P onset.

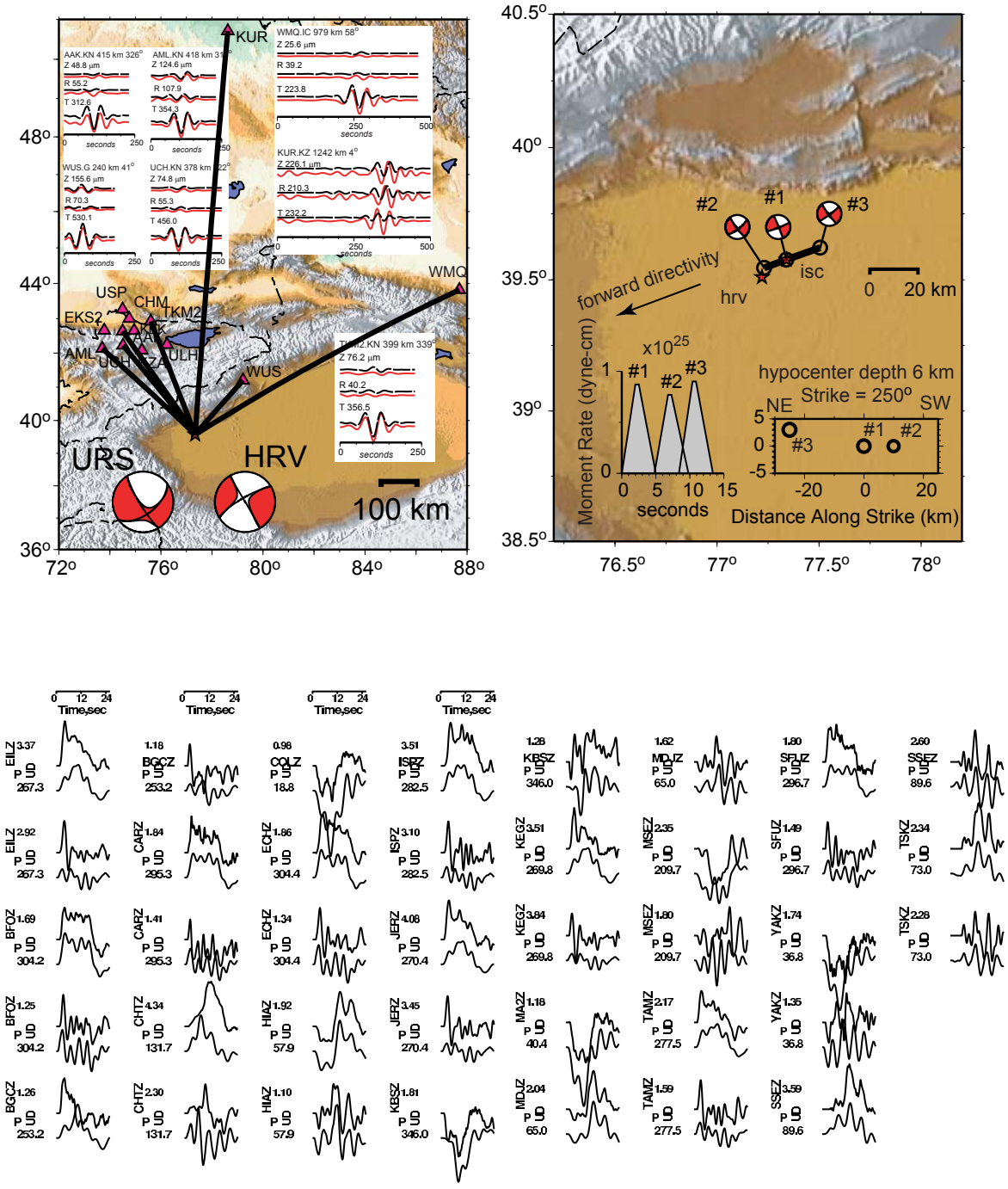

Figure 7. Top left panel shows regional moment tensor inversion (RMTI) results for the August 27, 1998 southern Xinjian Province, China earthquake. Three component long-period data from 7 regional stations were used to estimate the moment tensor solution, and its origin time and centroid depth. The top right panel shows the multiple point sources used in inversion including the results of teleseismic P wave inversion (bottom panel) using the "Kikuchi-method". This modeling is based on three point sources, a triangle shaped moment rate function and a fixed rupture velocity.